Journal of Materials Chemistry A

Accepted Manuscript

This is an *Accepted Manuscript*, which has been through the Royal Society of Chemistry peer review process and has been accepted for publication.

Accepted Manuscripts are published online shortly after acceptance, before technical editing, formatting and proof reading. Using this free service, authors can make their results available to the community, in citable form, before we publish the edited article. We will replace this *Accepted Manuscript* with the edited and formatted *Advance Article* as soon as it is available.

You can find more information about *Accepted Manuscripts* in the Information for Authors.

Please note that technical editing may introduce minor changes to the text and/or graphics, which may alter content. The journal's standard Terms & Conditions and the Ethical guidelines still apply. In no event shall the Royal Society of Chemistry be held responsible for any errors or omissions in this *Accepted Manuscript* or any consequences arising from the use of any information it contains.

ROYAL SOCIETY OF CHEMISTRY

www.rsc.org/materialsA

Turning periodic mesoporous organosilicas selective to CO_2/CH_4 separation: deposition of aluminium oxide by atomic layer deposition

Mirtha A. O. Lourenço[a], Ricardo M. Silva[a], Rui F. Silva[a], Nicola Pinna[b], Stephane Pronier[c], João Pires[d], José R. B. Gomes[e], Moisés L. Pinto[f], Paula Ferreira[a*]

[a] CICECO, Department of Materials & Ceramic Engineering, University of Aveiro, Campus Universitário de Santiago, 3810-193 Aveiro, Portugal
[b] Institut für Chemie, Humboldt-Universität zu Berlin, Brook-Taylor-Str. 2, 12489 Berlin, Germany
[c] Service Measures Physiques (IC2MP), University of Poitiers, CNRS, UMR7285, 4 rue Michel Brunet, 86022 Poitiers, France
[d] Center of chemistry and biochemistry, Faculdade de Ciências, Universidade de Lisboa, 1749-016 Lisboa, Portugal
[e] CICECO, Department of Chemistry, University of Aveiro, Campus Universitário de Santiago, 3810-193 Aveiro, Portugal
[f] CERENA, Instituto Superior Técnico, Universidade de Lisboa, Av. Rovisco Pais, n° 1, 1049-001 Lisboa, Portugal

Corresponding author: Paula Ferreira, email: pcferreira@ua.pt; phone: +351 234401419; fax: +351 234401470

Abstract

Nowadays, CO_2/CH_4 separation is considered extremely important to turn biogas economically interesting. The search of efficient materials for biogas upgrading is at the cutting edge of research in the field of energy. Periodic mesoporous organosilicas (PMO) have high potential to be applied as selective adsorbents for CO_2 as they have concomitant high specific surface areas and tunable surface properties. Here we describe the tuning of the surface properties of phenylene-PMO by using atomic layer deposition (ALD) to add active aluminium species to the walls of these organic-inorganic hybrid materials. The modification with aluminium oxide was attained with varying number of deposition cycles (from 2 to 100 cycles). A clear correlation between the amount of aluminium attached to PMO and the number of deposition cycles is observed. Consequently, the increase in the number of deposition cycles resulted in a reduction of the specific surface area and the pore volume of the PMO material. The variation of the number of deposition cycles to modify the surface of the PMOs yields composite materials with aluminium sites having different local coordination, but keeping intact the meso- and molecular-scale periodicity orders of the parent PMO. Adsorption results indicate that high selectivity for CO_2/CH_4 separation is

Journal of Materials Chemistry A Accepted Manuscript

obtained when pentacoordinated (Al^{V}) and tetrahedral (Al^{IV}) aluminium oxide are present in the PMO.

Keyword:
Periodic mesoporous organosilicas, PMO, ALD, CO_2/CH_4 separation

Introduction

Carbon dioxide is the major contaminant presented in biogas production and is also an important cause for global warming. Currently, the capture of CO_2 is performed by the use of monoethanol amine (MEA), which is a chemical solvent. This process demands high energy costs due to the need of solvent regeneration, and it has also associated corrosion problems. [1,2] In order to find an alternative method for CO_2 separation, researchers have devoted their attention to porous materials in the last decades.[3] Activated carbon[4], zeolites [2] and metal organic frameworks (MOFs)[5,6], were proposed as adsorbents for selective CO_2 uptake. However the performance of these adsorbents is so far not satisfactory. The ideal adsorbent for CO_2 capture must be highly selective and possess high adsorption capacity, acceptable adsorption/desorption kinetics, keep stable after several adsorption/desorption cycles, and be thermally and mechanically stable.[7] Periodic mesoporous organosilicas (PMOs) have been proposed for this aim due to their high specific surface areas, narrow distribution of pore sizes and high pore volumes.[8–10] Furthermore, PMOs with phenylene-bridge (from now on simply denoted as PMO) can be easily modified to turn its surface selective to CO_2.[11–14] So far the enhancement on the selectivity of porous materials towards CO_2 has mainly been attempted by organic modifications.[5,15–21] Zeolites and MOFs with aluminium (Al) open centre incorporated into their matrix structure have shown to improve the adsorption of CO_2.[22–28] To the best of our knowledge, the preparation of PMO/Al_2O_3 composites was never tried. Here, we describe for the first time the use of atomic layer deposition (ALD) to modify the PMO surface with Al_2O_3 in order to design a novel CO_2 adsorbent. ALD comprises a sequence of self-limiting chemical reactions between gas-phase precursor molecules and the solid surface. The self-limiting nature of ALD gives rise to a conformal growth and an additional control over the total stack thickness. The film

Journal of Materials Chemistry A Accepted Manuscript

thickness in a planar substrate can be determined precisely by the number of coating cycles.[29] In this work, by varying the number of ALD deposition cycles, the quantity of aluminium oxide deposited as well as the type of aluminium species on the PMO were studied.

Experimental details

PMO synthesis

The mesoporous phenylene bridged PMO was synthesized according to the literature procedures with slight modifications.[8,30,31] The synthesis of PMO started with the hydrolysis and condensation of 1,4-bis(triethoxysilyl)benzene (BTEB, 4.78 g)[32] precursor in the presence of octadecyltrimethylammonium bromide surfactant template (ODTMA, 4.8 g, Aldrich, 98%) in 124 mL of distilled water with 8 mL of 6 M NaOH solution. This solution was kept for 20 minutes in an ultrasonic vessel and stirred for 24 hours at room temperature. After 24 hours of ageing, the solution was transferred to Teflon-lined stain-steel autoclave for hydrothermal treatment. The hydrothermal treatment begins with a pre-heating of the autoclave in an oven at 200 ºC during 40 minutes, and then it was transferred to another oven at 100 ºC. After 24 hours, the solid was filter and washed. The template was extracted by an ethanol/HCl solution.

Al_2O_3-PMO preparation

ALD was performed with a cross flow home-made reactor working in continuous mode, using water and trimethylaluminium (Sigma Aldrich, 97%) as precursors. The precursors were alternately introduced through ALD pneumatic valves from their reservoirs, which were kept at room temperature. Alumina (Al_2O_3) was deposited onto the PMO at 200 °C, under 100 sccm of N_2 flow, using reactant pulse times of 0.05 s and 0.10 s for water and trimethylaluminium, respectively, and 30 s between pulse times. The typical operating pressures varied from 1.6 to 2.0 Pa during the precursor pulses. The quantity of Al_2O_3 deposited by ALD onto the PMO was determined by direct measurements performed before and after the ALD coating using an analytical balance with a precision of 0.1 mg.

Journal of Materials Chemistry A Accepted Manuscript

The resultant composite materials are denoted from now on as Al-PMO#*x*, where *x* corresponds to the number of deposition cycles.

An additional sample, PMO+Al_2O_3_a was prepared by physical mixture of PMO and amorphous Al_2O_3. The amorphous alumina was synthetized according to the literature[33] with some experimental modifications. The aluminium isopropoxide (Al(O*i*Pr), Aldrich, 1 g) was solubilized in ethanol (EtOH, PA, Carlo Erba Reagents, 9.75 mL). Then, 0.46g of nitric acid (HNO_3, 65 %, Panreac) was added to the solution, and the solution was vigorous stirred overnight at room temperature (RT). Then, the solution was transferred to an oven for 2 days at 60 ºC to induce the controlled evaporation of the solvent and to obtain the dry material. The obtained material was calcined at 400 ºC during 4 h with a heating ramp of 5 ºC·min^{-1}.

Materials characterization

The physical, textural and chemical properties of the pristine PMO and Al-PMO composites were evaluated by scanning electron microscopy (SEM), scanning transmission electron microscopy (STEM), powder X-ray diffraction (PXRD), low temperature (-196 ºC) nitrogen adsorption-desorption isotherms, transmission electron microscopy (TEM), Fourier transform infra-red (FTIR), ^{29}Si magic-angle spinning (MAS) and cross polarization (CP) MAS nuclear magnetic resonance (NMR), ^{13}C CP MAS and ^{27}Al MAS NMR spectroscopies. The thermal stability of materials was evaluated by thermogravimetry analysis (TGA). Description of the experimental conditions is presented at the Electronic Supplementary Information (ESI).

High pressure adsorption of CO_2 and CH_4

Adsorption experiments of CO_2 and CH_4 on selected samples were conducted up to 1000 kPa at 25 °C, using the volumetric method. These experiments were carried out on a lab made stainless steel volumetric apparatus, with a pressure transducer (Pfeiffer Vacuum, APR 266), and equipped with a vacuum system that allows a vacuum better than 10^{-2} Pa. The temperature was controlled with a stirred thermostatic water bath (Grant Instrument, GD-120) and before every experiment the samples were degassed for 2.5 h at 200 °C. The

Journal of Materials Chemistry A Accepted Manuscript

non-ideality of the gas phase was taken into account by using the second and third virial coefficients, and the experimental excess adsorbed amounts were converted to the absolute adsorbed amounts by taking into account the porous volume of the material and the density of the gas phase using the virial coefficients. Selectivity values were estimated using a method proposed by Myers[34] and the implementation is described in detail in previous works[35].

Results and Discussion

The influence of ALD deposition cycles on the morphological changes of PMO was investigated with a particular focus on the decrease of the surface area and pore volume. A series of Al_2O_3 depositions onto the PMO were performed using different number of cycles (2, 10, 20, 50 and 100 cycles). Weight gain measurements were performed on 25 mg PMO samples after the ALD coating to establish a relation with the number of cycles and the quantity of Al_2O_3 (here denoted as Al) deposited as shown in Table 1. This table shows that the weight gain increases with the number of coating cycles.

Table 1. Weight gain measurements between 0 and 100 Al_2O_3 ALD cycles and Si/Al ratios determined by EDS.

Sample	*Weight* / mg	*Δ weight / mg*	$[Si/Al]_{EDS}$
PMO	25.0	-	0
Al-PMO#2	n.m.[a]	n.m.[a]	n.m.[a]
Al-PMO#10	28.7	+ 3.7	10.47
Al-PMO#20	31.8	+ 6.8	2.54
Al-PMO#50	32.6	+ 7.6	1.87
Al-PMO#100	35.3	+ 10.3	0.94

[a]not measured

The Si/Al ratios determined by EDS (Table 1) reveal that the Al contents in the PMO increase with the number of applied ALD cycles. The difference between these values proves that the ALD precursors modified the pristine PMO material. It is interesting to note that Si/Al ratio does not decrease linearly with the weight gain.

The top surface morphology of the PMO coated with Al_2O_3 after 50 ALD cycles, i.e., Al-PMO#50 sample, was analysed from SEM and STEM bright field images (Fig. 1a,

Journal of Materials Chemistry A Accepted Manuscript

b) and corresponding EDS elemental mapping, which show the homogeneous distribution at µm-scale of both aluminium and silicon on the composite (Fig. 1c, d).

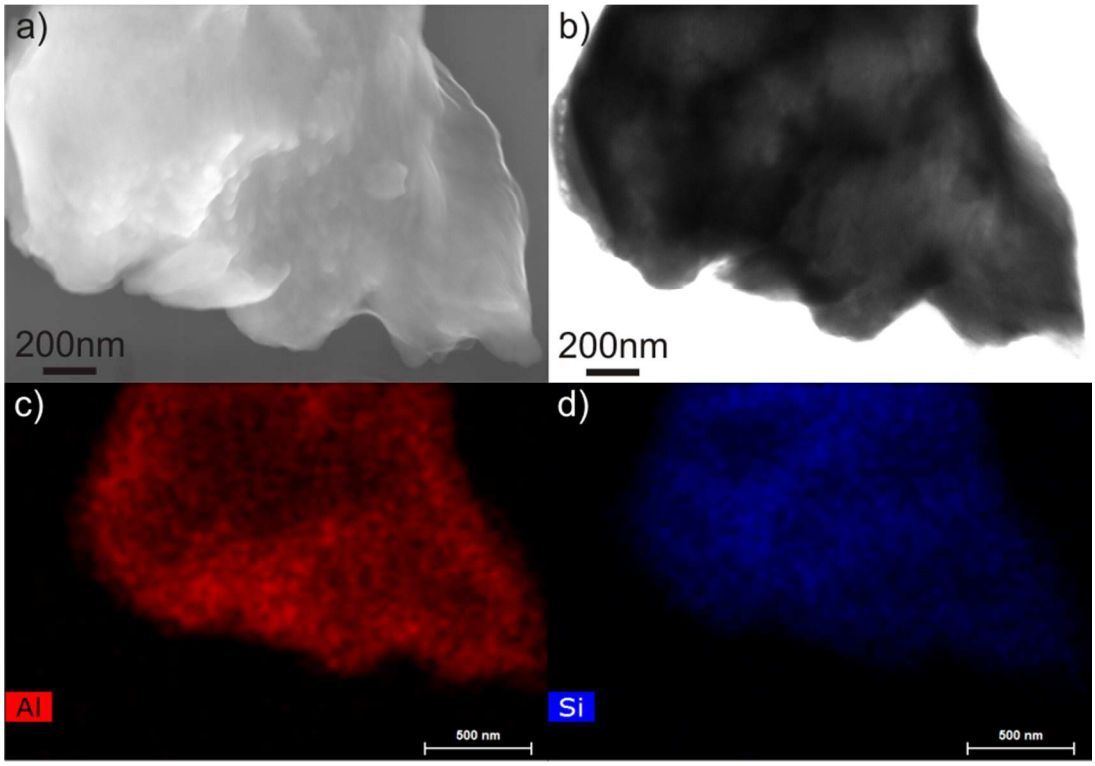

Figure 1. a) SEM and b) STEM bright field micrograph images of Al-PMO#50. The elemental map reveals the homogeneous distribution of aluminium (c) and the silicon (d).

PXRD patterns of PMO, Al-PMO#2, Al-PMO#10, Al-PMO#20, Al-PMO#50 and Al-PMO#100, (Figure 2) show the two-dimensional hexagonal symmetry (*p6mm*) lattice for all materials due to the presence of the first strong low-angle (100) reflection with d_{100} = 4.82 nm and the two much less intense (110) and (200) peaks. It is possible to observe in Figure 2 the decrease of intensity of the peaks with the increase of the number of Al_2O_3 deposition cycles. In addition, Figure 2 and numerical values in Table 2 display a slight shift to higher angles in the d_{100} diffraction peak as the number of deposition cycles increase. The peak at d = 0.762 nm corresponds to the molecular-scale crystal-like structure. The reduction in the intensity of this peak is also observed upon modification by Al_2O_3. A slight shift to higher angles is again observed. Peaks associated to both meso- and molecular- scale periodicities are preserved after modification suggesting that the PMO structure is not affected by the ALD conditions.

Journal of Materials Chemistry A Accepted Manuscript

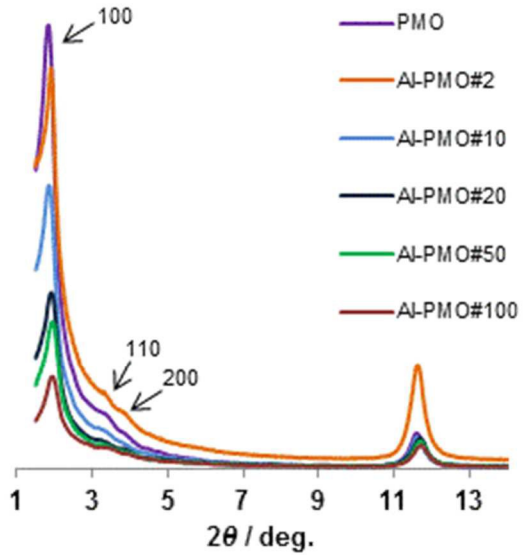

Figure 2. X-ray diffraction patterns of PMO, Al-PMO#2, Al-PMO#10, Al-PMO#20, Al-PMO#50 and Al-PMO#100.

For CO_2 adsorption application, it is of crucial importance that the pores are still accessible after ALD modification. The low temperature (-196 ºC) nitrogen adsorption–desorption isotherms and pore size distribution (PSD) curves (Table 2 and Figure S2, ESI) confirm the type IV isotherms (IUPAC classification) for PMO and ALD modified PMO with narrow distribution of pore sizes, typically observed for conventional mesoporous materials such as MCM-41, with a hexagonal structure. After 100 cycles of Al_2O_3 deposition, a significant decrease in the N_2 adsorbed amounts is observed. This may indicate that some of the pores are clogged.

Table 2. Physical properties of PMO, Al-PMO#2, Al-PMO#10, Al-PMO#20, Al-PMO#50 and Al-PMO#100.

Sample	d_{100} / nm	a / nm[a]	S_{BET} / m^2 g^{-1}	V_P / cm^3 g^{-1}	d_P / nm[b]
PMO	4.82	5.57	971	1.25	3.85
Al-PMO#2	4.65	5.36	645	0.79	3.81
Al-PMO#10	4.72	5.45	648	0.52	3.82
Al-PMO#20	4.62	5.34	513	0.39	3.74
Al-PMO#50	4.57	5.28	445	0.34	3.73
Al-PMO#100	4.53	5.23	204	0.18	3.74

[a]Unit cell parameter calculated as ($a = 2d_{100}/\sqrt{3}$). [b]Pore width obtained from the maximum on the BJH pore size distribution calculated on the basis of adsorption data.

Table 2 reveals a sharp decrease of the surface area and pore volumes with the growth of the amount of ALD Al (approximately linear). The slight decrease in the pore

Journal of Materials Chemistry A Accepted Manuscript

diameter may indicate that just a little amount of Al_2O_3 is deposited inside the pores. From our results, the Al_2O_3 is mostly deposited on the top surface area of the particles leading to partial clogging of the pores. This effect was most pronounced for the sample Al-PMO#100.

The TEM cross-section image and corresponding EDS analyses of the pristine PMO and the composites Al-PMO#2, Al-PMO#50 and Al-PMO#100 are shown in Figures 3 and S3. The collected images show the hexagonal arrangement of the pores for all materials suggesting that the Al modification using ALD technology is not contributing to disrupt of the pore structure of the parent PMO (Figure 3), which is in agreement with the PXRD diffractograms (cf. Figure 2). Additionally, it is also possible to observe the mass contrast in the images of the Al-PMO composites. The darker zones correspond to the Al content inserted into the pores or present at the surface of the materials, Figures 3 (Al-PMO#100) and S3 (ESI). TEM EDS analyses seem to indicate a low degree of aluminium impregnation inside the pores of the PMO. The aluminium oxide is mostly deposited at the external surface of the particle for all composite materials, Figure S3 (ESI). This behaviour is more evident for the composite materials obtained with larger number of deposition cycles, e.g. Al-PMO#50 and Al-PMO#100. The insets illustrate the FFT of hexagonal arrangement of the pores of the composites.

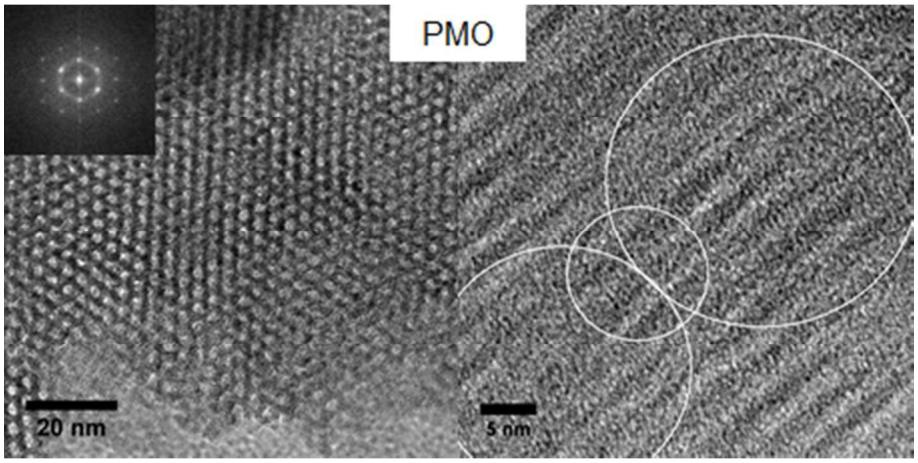

Journal of Materials Chemistry A Accepted Manuscript

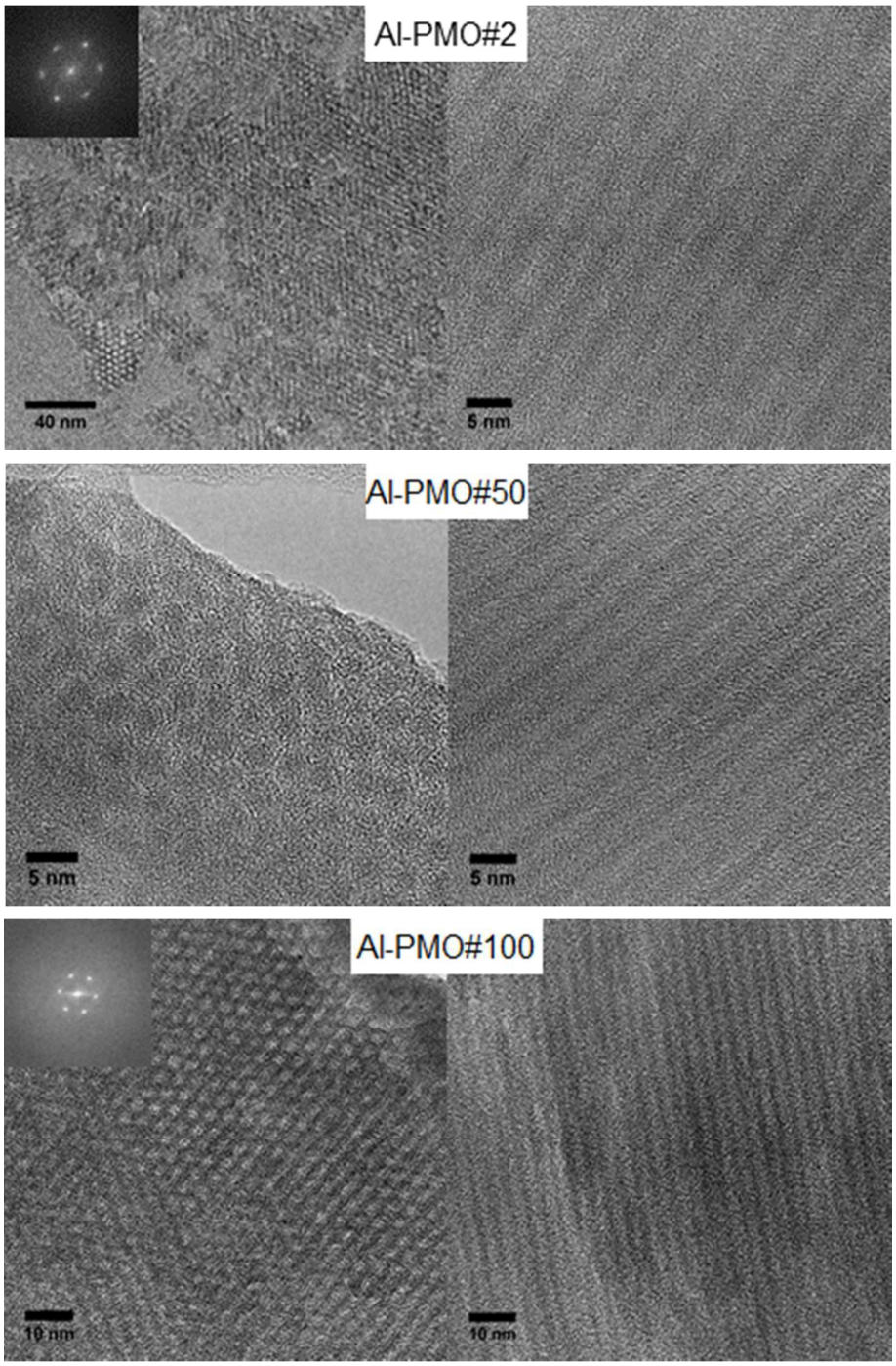

Figure 3. TEM cross-section images of PMO, Al-PMO#2, Al-PMO#50 and Al-PMO#100. In the left side is presented typically the view parallel to the porous channels, while the right side shows the view perpendicular to the channels. The circles in the top-right panel are used to better illustrate the molecular-scale periodicity. The insets show the FFT of the hexagonal arrangement of the pores.

Journal of Materials Chemistry A Accepted Manuscript

Different techniques were employed for evaluating if any change in the chemistry of the material occurs upon the modification of the PMO material with different amounts of Al_2O_3. The spectra (Figure S4a) obtained with Fourier transform infrared spectroscopy (FTIR) show that the PMO parent material displays adsorption bands assignable to the phenylene ring vibrations (1300–2000 cm^{-1}) and strong adsorption bands (900-650 cm^{-1}), C–H species (2980-3060 cm^{-1}, Figure S4b), and stretching modes of silanol (3632 cm^{-1}, Figure S4b). The increase of the amount of Al_2O_3 deposited in the pristine PMO is observed in the FTIR spectra by the reduction of the intensity of the bands between 350 and 1200 cm^{-1}. The ^{29}Si and ^{13}C CP MAS NMR spectra of Al_2O_3-PMO#50 (Figure S5 and Figure S6) were also collected for comparison with the already described pristine PMO.[30] ^{29}Si CP MAS NMR spectrum of Al-PMO#50 exhibits the typical peaks at *ca.* -81, -72 and -61 ppm attributed to T^3, T^2 and T^1 [T^m = $RSi(OSi)_m(OH)_{3-m}$] organosiliceous species, respectively, without any alteration comparing with the parent material.[13,30] The material obtained from deposition of Al_2O_3 by ALD at 200 °C does not present resonances in the region of the Q^n species [Q^n = $Si(OSi)_n(OH)_{4-n}$] proving that the C-Si bonds are intact. Table S1 shows the percentages of T^m species in PMO and Al-PMO#50. These percentages are calculated from the deconvolution of the ^{29}Si MAS NMR spectra, using the common assumption of Gaussian distributions of isotropic chemical shifts for each type of T^m specie. Usually, the overlapping of T^m resonances is noticed, leading to small variations between best-fit intensity parameters and, consequently, to uncertainties associated with the relative populations of the T^m sites. The degree of condensation is 59% for the PMO and 64% for the Al-PMO#50 composite. The increase of approximately 5% in the T^3 silicon species and the reduction of T^2 site in the Al-PMO#50 composite are probably due to some condensation of alumina to the free hydroxyl group of the T^2 silicon environment of the PMO. Furthermore, ^{13}C CP MAS NMR spectrum supports the preservation of the material chemistry displaying only one peak at *ca.* 133 ppm that is assigned to the carbons of the phenylene bridge. ^{27}Al MAS NMR spectrum (Figure 4) shows the presence of three peaks at 5, 38 and 62 ppm assigned to the Al^{VI} octahedral, Al^{V} bipyramidal and Al^{IV} tetrahedral coordinated aluminium, respectively. Note that the Al_2O_3 deposited by ALD is amorphous. However, the tetrahedral and the bipyramidal Al-sites can promote acidity in the material. This property can allow the use of Al-PMO composites in CO_2 / CH_4 separation once

Journal of Materials Chemistry A Accepted Manuscript

promotes the interaction between composite and the CO_2 quadrupole and consequently improves the selectivity.

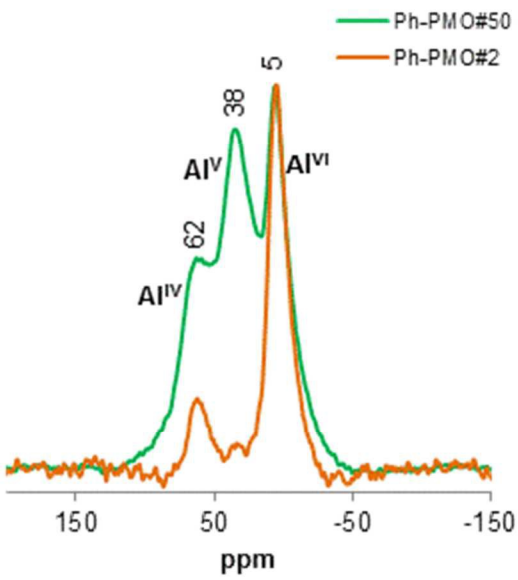

Figure 4. ^{27}Al MAS NMR spectra of Al-PMO#2 and Al-PMO#50.

Figure 4 also shows the ^{27}Al MAS NMR spectrum of the Al-PMO#2 composite. This material presents two main distinct peaks, which are assigned to the Al^{VI} octahedral and Al^{IV} tetrahedral coordinated aluminium species. A third peak attributed to pentacoordinated aluminium species (Al^{V}) grows in importance with the increase of the number of cycles, which is a sign of the formation of defects.

The TGA curve of Al-PMO#50 (Figure S7) exhibits a first weight loss below 100 °C due to desorption of physisorbed water. It is possible to observe a 3% weight loss from 100 to 250 °C due to the presence of a small quantity of non-extracted template. At 400 and 630 °C, it is possible to observe two weight losses of 23% due to the decomposition and release of the organic moieties from the bridges of the PMO material. Note that pristine PMO material presents a thermal stability up to 550 °C and above that temperature only one weight loss is observed.[12,13,30] Thus, the introduction of the Al content decreases the thermal stability of the material. This means that the degradation of the organic content is aided by the deposited Al_2O_3 in two steps due to the presence of different types of Al coordination. The first step of degradation of the phenylene bridges occurs probably due to the contact of infiltrated pentacoordinated alumina (Al^{V}) with the organic moieties of the

Journal of Materials Chemistry A Accepted Manuscript

PMO. The other weight loss at 630 °C corresponds to the degradation and release of the remaining phenylene moieties. These organic moieties probably are in contact with the octahehedral alumina (Al^{VI}). Note that this temperature of degradation is superior to the temperature needed to promote the degradation of phenylene bridges of the pristine PMO (550 ºC). This picture is supported by the larger stability of the Al^{VI} species which presumably protect the organic bridges in their vicinity with a concomitant increase in their thermal stability.

High pressure adsorption of methane and carbon dioxide was performed on samples Al-PMO#50, Al-PMO#2 and parent PMO. These PMOs modified with ALD were chosen because they presented different properties as above discussed, but they still maintained a significant surface area and pore volume (Table 2). The adsorbed amounts on the samples modified with ALD (Al-PMO#50, Al-PMO#2) decreased for both carbon dioxide and methane (Figure 5). It can be noted that the decreasing is more pronounced on the sample treated with more ALD cycles (Al-PMO#50). This is expected taking into account the significant decrease in pore volume comparing with that determined for the parent PMO (about 60%, Table 2). However, the decrease in the adsorbed amounts is different for carbon dioxide and methane. Comparing the isotherms for PMO and Al-PMO#50, it becomes clear that the decrease is less pronounced with carbon dioxide, probably because of the specific interaction of this molecule with the surface of the materials. In fact, we have fitted the isotherm data with a virial equation (lines in Figure 5; parameters in Table 3) and observed that the Henry constant (K), which is sensitive to the interaction of the molecules with the surface of the materials, increases with the number of ALD cycles for the carbon dioxide case and conversely decreases for the methane case. This indicates that the surface of the PMO is increasing the affinity for carbon dioxide with the number of ALD cycles, while the contrary is observed for methane. Another way to ascertain this increase is to represent the adsorbed amounts per surface area of the materials (A_{BET}) instead of mass, in order to take into account the decrease of the surface observed due to ALD treatment and to normalize the results by surface affinity. These results (Figure S8) clearly show a significant increase of about two times from PMO to Al-PMO#50 in the adsorbed amount of carbon dioxide per surface area when more Al_2O_3 is introduced in the

Journal of Materials Chemistry A Accepted Manuscript

pores of PMO. This change has a dramatic impact on the separation properties of the materials as we will discuss below.

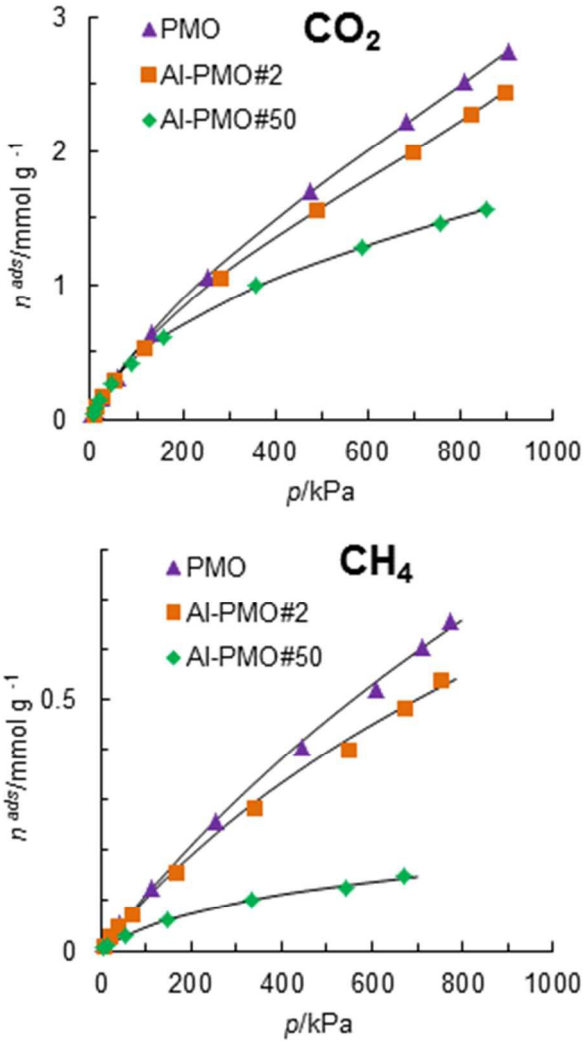

Figure 5. Carbon dioxide and methane adsorption isotherms at 25ºC on the PMO, Al-PMO#2 and Al-PMO#50. The lines represent the fitting of the virial equation.

Journal of Materials Chemistry A Accepted Manuscript

Table 3. Virial coefficients (C_1 and C_2) and Henry constants (K) for the adsorption of methane and carbon dioxide on the pristine and modified PMOs.[a]

Gas	Material	K	C_1	C_2
		mol kg^{-1} kPa^{-1}	kg mol^{-1}	(kg mol^{-1})^2
CH_4	PMO	1.17×10^{-3}	0.536	
	Al-PMO#2	1.14×10^{-3}	0.935	
	Al-PMO#50	0.674×10^{-3}	7.853	
	PMO+Al_2O_3_a	0.467×10^{-3}	-0.319	
CO_2	PMO	6.41×10^{-3}	0.474	-0.074
	Al-PMO#2	7.03×10^{-3}	0.730	-0.141
	Al-PMO#50	8.47×10^{-3}	1.429	-0.286
	PMO+Al_2O_3_a	0.86×10^{-3}	-0.613	0.111

[a] Obtained by the nonlinear least-squares the virial equation to the adsorption data

Using the virial equation fitted to the adsorption data and the Ideal Adsorbed Solution Theory (IAST),[36] the selectivity of the separation and the equilibrium phase diagrams for the adsorbed phase can be obtained using a method proposed by Myers[34] with the implementation described in detail in previous works[35,37] As can be seen from Figure 6, the inclusion of Al_2O_3 on the PMO induces a very significant increase in the selectivity of the CO_2/CH_4 separation, i.e., the Al-PMO#50 case is much more pronounced than the Al-PMO#2. This is most probably related with the aluminium pentacoordinated species (Al^V) that are present in large amount in the Al-PMO#50 and almost absent in Al-PMO#2. This type of aluminium oxide species is very acidic[38,39] and can interact strongly with the carbon dioxide quadrupolar moment (3.3×10^{-16} cm^2).[40] It is worth mentioning that the selectivity values found for the CO_2/CH_4 separation on Al-PMO#50 sample are similar to those found on some pillared clays with aluminium oxide pillars.[35,37]

Journal of Materials Chemistry A Accepted Manuscript

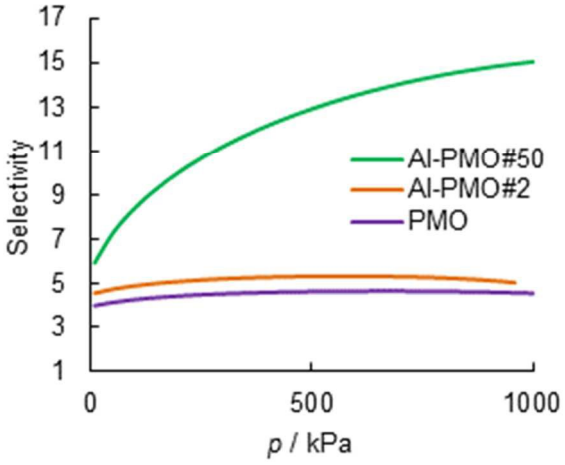

Figure 6. Average selectivity for the CO_2/CH_4 separation on the pristine and modified PMOs.

The influence on the separation can be best illustrated in Figure 7 where it can be seen that the sample Al-PMO#50 has an improved performance over the other samples. If we consider a sample with 0.5 molar composition (y_{CH4}), typical of biogas composition and some natural gas sources, the composition in the adsorbed phase (x_{CH4}) is 0.15 on PMO, 0.13 on Al-PMO#2 and 0.02 at Al-PMO#50, at 500 kPa and 25 ºC. This means that the adsorbed phase is richer in carbon dioxide than in methane and that Al-PMO#50 adsorbs almost pure carbon dioxide (0.98 molar composition) under these conditions. Complete phase diagrams can also be obtained (Figure S9), which confirm the best performance of the Al-PMO#50 sample. Thus, the small decrease in adsorption capacity due to the ALD treatment is largely compensated by the increase in the selectivity.

Journal of Materials Chemistry A Accepted Manuscript

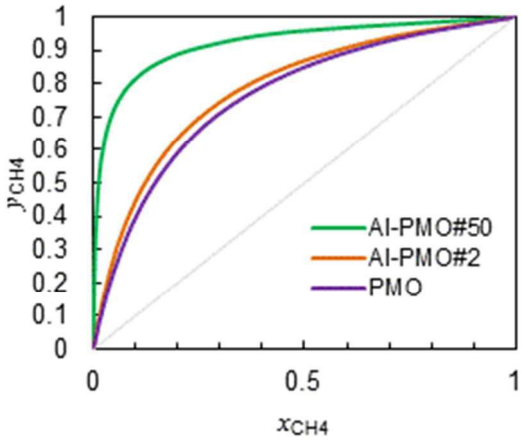

Figure 7. Isothermal (25ºC), isobaric (500 kPa) *xy* phase diagrams of the CO_2/CH_4 mixtures on the pristine and modified PMOs. y_{CH4} is the molar faction of methane in the gas phase; x_{CH4} is the molar faction of methane in the adsorbed phase.

The application of adsorbent materials on the separation of gases is only industrially viable if the material can be easily regenerated with minimum loss of capacity after each regeneration cycle. We have tested the regeneration possibility on the Al-PMO#2 and Al-PMO#50 composites using just vacuum during half hour at ambient temperature. This corresponds to what happens industrially during the regeneration step of a vacuum swing adsorption process (VSA).[41] From the presented results (Figure 8), only a slight decrease in the high pressure region can be noted in both composites, although more significant in Al-PMO#50. This is a first good indication that these materials can be easily regenerated and that they are stable to be used under cyclic separation processes. Additional confirmation using a higher number of cycles would be needed to confirm the stability required for application in industry.

Journal of Materials Chemistry A Accepted Manuscript

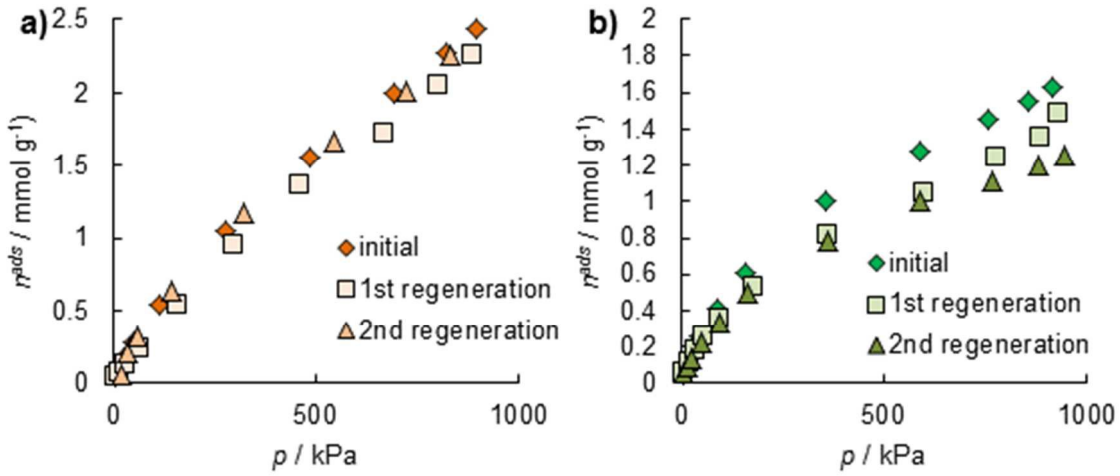

Figure 8. Adsorbed amounts of the CO_2 in a) Al-PMO#2 and b) Al-PMO#50 after first and second regeneration steps of the composites with vacuum at 25 ºC during half hour.

The advantage of impregnating Al_2O_3 on the PMO using ALD is also evaluated through the comparison of Al-PMO#50 composite and the physical mixture of PMO with amorphous alumina powder regarding the CO_2 and CH_4 adsorption. For a more realistic comparison, the amorphous alumina used presents a similar chemical composition to that of Al-PMO#50 (see Figure S10). In addition, the physical mixture of PMO and amorphous alumina is made in the same ratio obtained for the Al-PMO#50 composite. This is possible having into account the weight gain presented in Table 1. The mixture of PMO with amorphous alumina is here denoted as PMO+Al_2O_3_a and was tested for the CH_4 and CO_2 adsorption at 25 ºC.. It is possible to observe that PMO+Al_2O_3_a adsorbs a smaller amount of CO_2 and a larger quantity of CH_4 when compared with Al-PMO#50 (Figure S11a). The presence of nearly 25% of amorphous alumina induces a negative effect in the CO_2 adsorption in the PMO. In addition the selectivity for PMO+Al_2O_3_a, presented in Figure S11b, is about 1.86 at 500 kPa, while the PMO presents a selectivity of approximately 4 and the Al-PMO#50 presents a selectivity of 13 at the same range of pressure. Furthermore the PMO+Al_2O_3_a showed the worst separation performance among all materials (Figure S12a) and the equimolar composition in the adsorbed phase is achieved at about 0.70 molar composition of methane in the gas phase, at 500 kPa and 25 ºC (Figure S12b), which is significantly lower than those observed for the other materials tested. Having into account

Journal of Materials Chemistry A Accepted Manuscript

the performance of PMO+Al_2O_3_a material on the CO_2 adsorption, the presence of the same alumina/PMO ratio and same chemical composition achieved for the Al-PMO#50, it is possible to conclude that the use of ALD to deposit alumina in the PMO powder brings benefits for the CO_2/CH_4 separation. This can be due to a good dispersion of nanoparticles of amorphous alumina that is achieved with the ALD method not only in the surface, but also inside the pores of Al-PMO#50, probably promoting some roughness and microporosity. The interactions of the alumina and the gas molecules are then increased, since the alumina particles are very small. Another consequence of this type of deposition is the eventual chemical reaction of some alumina with some of the T^2 free silanols of PMO giving rise to some Si-O-Al chemical bonds. In this way, the ALD allows the deposition of amorphous alumina on the PMO, in order to produce composites with interesting physical and chemical characteristics to be selective in the CO_2 / CH_4 separation.

Comparison to other materials

The capacity of Al-PMO#50 to capture carbon dioxide and methane is compared in Table 4 with the capacities reported for other types of adsorbents. Notice that data were determined at different temperatures, thus, some differences on the values of the capacities can be due to the temperature.

Table 4. Capacities of different adsorbents in the CO_2 / CH_4 separation at 100 kPa.

Type	Materials	CO_2 capacity ($mol \cdot kg^{-1}$)	CH_4 capacity ($mol \cdot kg^{-1}$)	Temperature	Selectivit[a]
Clays	PILC Al_w[35]	≈0.4	≈0.07	25ºC	≈12.0
	PILC Al_B[35]	≈0.4	≈0.08		≈10.0
	PCH[42]	≈0.7	≈0.08		≈7.0
Carbons	SC700P[43]	≈3.0	≈1.40		≈4.2
MOFs	amino-MIL-53(Al)[44]	1.96	≈0.30		6.5[b]
	MIL-53(Al) tablets (Basolite® A100)[45]	≈2.0	≈0.70	30ºC	≈3.0
Silicas	a-MCMBs[46]	12.4	6.10		≈1.9
ZIF	ZIF-7[47]	2.34	0.13	25ºC	≈18.0
PMOs	Al-PMO#50	≈0.5	≈0.04		≈9.0

[a]Selectivity at 100 kPa. [b] This value correspond to the CO_2/CH_4 capacity ratio.

Journal of Materials Chemistry A Accepted Manuscript

The Al-PMO#50 presents slightly better results in the CO_2 and CH_4 adsorption capacities than PILC-Al_B and $PILC_w$. The Al-PMO#50 presents at 100 kPa a selectivity of 9 which is lightly smaller than the selectivity reported for the PILCs at the same range of pressure. Although, the selectivity of the Al-PMO#50 increases with the pressure and at near of 1000 kPa these materials has a selectivity of 15 while the selectivity of these PILCs remains constant in the all range of pressure (100-1000 kPa). The Al-PMO#50 adsorbs less CO_2 than PCH clay, SC700P activated carbon, amino-MIL-53(Al) and MIL-53(Al) pellets (Basolite® A100) MOFs and a-MCMBs Silicas, but it is much superior in selectivity. The ZIF-7 is the only material that presents better CO_2 adsorption and selectivity at the same temperature and pressure. Although, information of the behaviour of these materials at higher pressures than 100 kPa is missing.

Conclusions

The phenylene-PMO surface was successfully modified for the first time by ALD deposition of amorphous Al_2O_3 with different content. The meso-structure order and molecular-scale periodicity of the pore walls of PMO are preserved after modification of high Al content (Al-PMO#100 with [Si/Al] = 0.94). The ALD method allows increasing the amount of the Al_2O_3 on the composite varying the number of cycles, proving to be a robust method for tailoring the content of Al_2O_3 amount on the PMO. The reduction of the surface area and pore volume is observed with the increase of Al content. For large number of cycles (50), the formation of Al^V aluminum oxide species is observed. The acidity of these species is most probably responsible for the observed increase in the CO_2/CH_4 separation selectivity. The Al-PMO#50 sample has interesting properties for application into methane purification (upgrading and sweetening) that is essential before bio and natural gas commercialization. The regeneration of the modified materials was easy under vacuum and showed good stability. The application of these materials as acidic catalysts is also anticipated.

Journal of Materials Chemistry A Accepted Manuscript

Acknowledgement

Authors are grateful to the Fundação para a Ciência e a Tecnologia (FCT), Fundo Europeu de Desenvolvimento Regional (FEDER), QREN-COMPETE, the European Union. This work was developed in the scope of the projects CICECO - Aveiro Institute of Materials, CERENA and CQB (FCT UID/CTM/50011/2013, UID/MULTI/00612/2013, UID/ECI/04028/2013, respectively), financed by national funds through the FCT/MEC and co-financed by FEDER under the PT2020 partnership agreement. PF, JRBG and MLP acknowledge the Investigador FCT program. FCT is also acknowledged by MLP for project IF/00993/2012/CP0172/CT0013 and by MAOL and RMS for the PhD grants with references SFRH/BD/80883/2011 and SFRH/BD/90844/2012, respectively.

Notes and References

† Electronic Supplementary Information (ESI) available. See DOI: xx.xxxx/bxxxxxxx/

1 G. Maurin, P. L. Llewelly and R. G. Bell, *J Phys Chem B*, 2005, **109**, 16084.

2 S.-T. Yang, J.-Y. Kim, J. Kim and W.-S. Ahn, *Fuel*, 2012, **97**, 435.

3 A. Garcia-Sanchez, C. O. Ania, J. B. Parra, D. Dubbeldam, T. J. H. Vlugt, R. Krishna and S. Calero, *J Phys Chem C*, 2009, **113**, 8814.

4 C. Y. Yin, M. K. Aroua and W. M. A. W. Daud, *Sep. Purif. Technol.*, 2007, **52**, 403–415.

5 A. Torrisi, R. G. Bell and C. Mellot-Draznieks, *Crystal Growth & Design,*, 2010, **10**, 7.

6 G. S. Bourrelly, P. L. Llewellyn, C. Serre, F. Millange, T. Loiseau, G. Ferey, *J. Am. Chem. Soc.*, 2005, **127**, 13519.

7 A. Walcarius and L. Mercier, *Journal of Materials Chemistry*, 2010, **20**, 4478–4511.

8 T. Asefa, M. J. MacLachlan, N. Coombs and G. A. Ozin, *Nature*, 1999, **402**, 867–871.

9 S. Inagaki, S. Guan, Y. Fukushima and T. Ohsuna, *J. Am. Chem. Soc.*, 1999, **121**, 9611–9614.

10 B. Melde, B. Holland, C. Blanford and A. Stein, *Chemistry of Materials*, 1999, 3302–3308.

11 M. Ohashi, M. P. Kapoor and S. Inagaki, *Chemical Communications*, 2008, **7**, 841–3.

12 M. Lourenço, R. Siegel, L. Mafra and P. Ferreira, *Dalton Trans.*, 2013, **42**, 5631–5634.

13 S. Inagaki, S. Guan, T. Ohsuna and O. Terasaki, *Nature*, 2002, **416**, 304–7.

Journal of Materials Chemistry A Accepted Manuscript

14 P. Ferreira, C. Bispo, M. A. O. Lourenço, J. R. B. Gomes, N. Bion, K. D. O. Vigier and F. Jérôme, in *Comprehensive guide for mesoporous materials, volume 4: application and commercialization*, ed. M. Aliofkhazraei, Nova Science Publishers, Inc., 2014, pp. 261–295.

15 A. Zukal, I. Dominguez, J. MayerovĂ and J. Čejka, *Langmuir : the ACS journal of surfaces and colloids*, 2009, **25**, 10314–21.

16 V. Zeleňak, M. Badaničova, D. Halamova, J. Čejka, A. Zukal, N. Murafa and G. Goerigk, *Chem Eng J*, 2008, **144**, 336.

17 C. Chen and W. S. Ahn, *Chem Eng J*, 2011, **166**, 646.

18 O. G. Nik, B. Nohair and S. Kaliaguine, *Micropor Mesopor Mater*, 2011, **143**, 221.

19 T. W. Pechar, S. Kim, B. Vaughan, E. Marand, M. Tsapatsis, H. K. Jeong, C. J. Cornelius, *J Membr Sci*, 2006, **227**, 195.

20 F. Su, C. Lu, S. C. Kuo, W. Zeng, *Energ. Fuel.*, 2010, **24**, 1441.

21 U. Martinez and G. Pacchioni, *Microporous and Mesoporous Materials*, 2010, **129**, 62–67.

22 Z. Zhou, Y. Qi, M. Xie, Z. Cheng and W. Yuan, *Chemical Engineering Science*, 2012, **74**, 172.

23 S. Biswas, T. Rémy, S. Couck, D. Denysenko, G. Rampelberg, J. F. M. Denayer, D. Volkmer, C. Detavernier and P. Van Der Voort, *Phys.Chem. Chem. Phys.*, 2013, **15**, 3552.

24 S.-H. Lo, C.-H. Chien, Y.-L. Lai, C.-C. Yang, J. J. Lee, D. S. Rajaa and C.-H. Lin, *J. Mater. Chem. A*, 2013, **1**, 324.

25 Q. Yang, S. Vaesen, M. Vishnuvarthan, F. Ragon, C. Serre, A. Vimont, M. Daturi, G. De Weireld and G. Maurin, *J. Mater. Chem.*, 2012, **22**, 10210.

26 X. Si, J. Zhang, F. Li, C. Jiao, S. Wang, S. Liu, Z. Li, H. Zhou, L. Sun and F. Xu, *Dalton Trans.*, 2012, **41**, 3119.

27 P. Rallapalli, K. P. Prasanth, D. Patil, R. S. Somani, R. V. Jasra, H. C. Bajaj, *Porous Mater*, 2011, **18**, 205.

28 X. Shang, X. Wang, W. Nie, X. Guo, X. Zou, W. Ding and X. Lua, *Journal of Materials Chemistry*, 2012, **22**, 23806.

29 M. Knez, K. Nielsch and L. Niinistö, *Advanced Materials*, 2007, **19**, 3425–3438.

30 N. Bion, P. Ferreira, A. Valente, I. S. Gonçalves and J. Rocha, *Journal of Materials Chemistry*, 2003, **13**, 1910–1913.

31 G. Smeulders, C. J. Van Oers, K. Van Havenbergh, K. Houthoofd, M. Mertens, J. A. Martens, S. Bals, B. U. W. Maes, V. Meynen and P. Cool, *Chemical Engineering Journal*, 2011, **175**, 585–591.

32 R. J. P. Corriu, J. J. E. Morea, P. Thepot and M. W. Chi Man, *Chem. Mater.*, 1992, **4**, 1217–1224.

Journal of Materials Chemistry A Accepted Manuscript

33 S. Hartmann, A. Sachse and A. Galarneau, *Materials*, 2012, **5**, 336–349.

34 A. L. Myers, *Adsorption*, 2003, **9**, 9–16.

35 J. Pires, V. K. Saini and M. L. Pinto, *Environmental Science & Technology*, 2008, **42**, 8727–8732.

36 A. L. Myers and J. M. Prausnitz, *AIChE Journal*, 1965, **11**, 121–127.

37 M. L. Pinto, J. Pires and J. Rocha, *J. Pys. Chem. C.*, 2008, **112**, 14394–14402.

38 G. Cre, V. Montouillout, A. Vimont, L. Mariey, T. Cseri and F. Mauge, 2006, 15172–15185.

39 L. Heeribout, R. Vincent, P. Batamack, C. Dor and J. Fraissard, 1998, **53**, 23–31.

40 R. W. Zwanzig, *The Journal of Chemical Physics*, 1956, **25**, 211.

41 R. T. Yang, *Gas Separation by Adsorption Processes*, Butterworths Publishers: Boston, 1987.

42 V. K. Saini, M. Pinto and J. Pires, *Green Chemistry*, 2011, **13**, 1251.

43 A. S. Mestre, C. Freire, J. Pires, A. P. Carvalho and M. L. Pinto, *Journal of Materials Chemistry A*, 2014, **2**, 15337.

44 S. A. Peter, G. V. Baron, J. Gascon, F. Kapteijn and J. F. M. Denayer, *Adsorption*, 2013, **19**, 1235–1244.

45 A. F. P. Ferreira, A. M. Ribeiro, S. Kulaç and A. E. Rodrigues, *Chemical Engineering Science*, 2015, **124**, 79–95.

46 X. Peng, W. Wang, R. Xue and Z. Shen, *AIChE Journal*, 2006, **52**, 994–1003.

47 X. Wu, M. Niknam Shahrak, B. Yuan and S. Deng, *Microporous and Mesoporous Materials*, 2014, **190**, 189–196.

Journal of Materials Chemistry A Accepted Manuscript

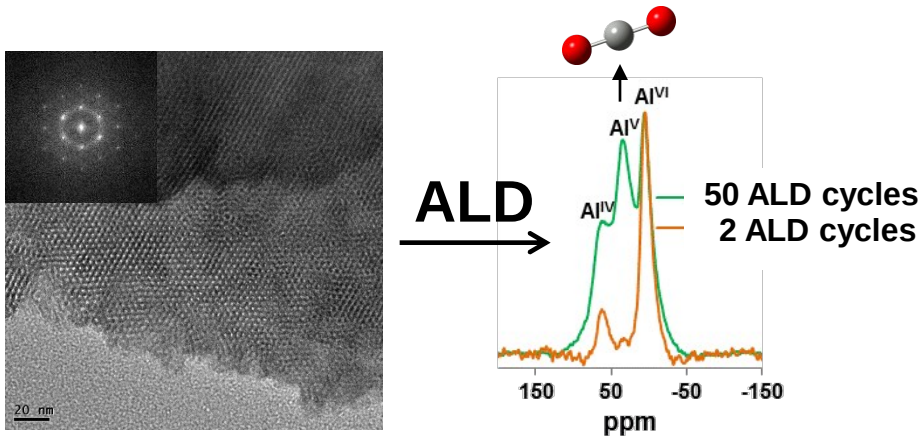

PMO **Al-PMO composite**

Journal of Materials Chemistry A Accepted Manuscript